
AFRL-RX-WP-TP-2011-4226

# CHARACTERIZATION OF FATIGUE CRACK-INITITATION FACETS IN RELATION TO LIFETIME VARIABLILITY IN Ti-6Al-4V (Preprint)

**Patrick Golden and Reji John**

**Behavior/Life Prediction Section**
**Metals Branch**

**Sushant Jha and Christopher Szczepanski**

**Universal Technology Corporation**

**William Porter, III**

**University of Dayton Research Institute**

**JULY 2011**



**AIR FORCE RESEARCH LABORATORY**
**MATERIALS AND MANUFACTURING DIRECTORATE**
**WRIGHT-PATTERSON AIR FORCE BASE, OH 45433-7750**
**AIR FORCE MATERIEL COMMAND**
**UNITED STATES AIR FORCE**

# REPORT DOCUMENTATION PAGE

*Form Approved*
*OMB No. 0704-0188*



| 1. REPORT DATE *(DD-MM-YY)* | 2. REPORT TYPE | 3. DATES COVERED *(From - To)* |
|---|---|---|
| July 2011 | Journal Article Preprint | 01 July 2011 – 01 July 2011 |

**4. TITLE AND SUBTITLE**

CHARACTERIZATION OF FATIGUE CRACK-INITITATION FACETS IN RELATION TO LIFETIME VARIABLILITY IN Ti-6Al-4V (Preprint)

**5a. CONTRACT NUMBER**
IN-HOUSE

**5b. GRANT NUMBER**

**5c. PROGRAM ELEMENT NUMBER**
62102F

**6. AUTHOR(S)**

Patrick Golden and Reji John (Metals Branch, Behavior/Life Prediction Section (AFRL/RXLMN))
Sushant Jha and Christopher Szczepanski (Universal Technology Corporation)
William Porter, III (University of Dayton Research Institute)

**5d. PROJECT NUMBER**
4349

**5e. TASK NUMBER**
20

**5f. WORK UNIT NUMBER**
LM110100

**7. PERFORMING ORGANIZATION NAME(S) AND ADDRESS(ES)**

Metals Branch, Behavior/Life Prediction Section (AFRL/RXLMN)
Materials and Manufacturing Directorate, Air Force Research Laboratory
Wright-Patterson Air Force Base, OH 45433-7750
Air Force Materiel Command, United States Air Force

Universal Technology Corporation
---
University of Dayton Research Institute

**8. PERFORMING ORGANIZATION REPORT NUMBER**
AFRL-RX-WP-TP-2011-4226

**9. SPONSORING/MONITORING AGENCY NAME(S) AND ADDRESS(ES)**

Air Force Research Laboratory
Materials and Manufacturing Directorate
Wright-Patterson Air Force Base, OH 45433-7750
Air Force Materiel Command
United States Air Force

**10. SPONSORING/MONITORING AGENCY ACRONYM(S)**
AFRL/RXLM

**11. SPONSORING/MONITORING AGENCY REPORT NUMBER(S)**
AFRL-RX-WP-TP-2011-4226

**12. DISTRIBUTION/AVAILABILITY STATEMENT**
Approved for public release; distribution unlimited.

**13. SUPPLEMENTARY NOTES**

PAO case number 88ABW-2010-5386 cleared 06 October 2010. This work was funded in whole or in part by Department of the Air Force work unit LM110100. The U.S. Government has for itself and others acting on its behalf an unlimited, paid-up, nonexclusive, irrevocable worldwide license to use, modify, reproduce, release, perform, display, or disclose the work by or on behalf of the U. S. Government. Submitted to the International Journal of Fatigue. Document contains color.

**14. ABSTRACT**

An analysis of fatigue crack-initiation facets from the perspective of variability in lifetime of a duplex microstructure of Ti-6Al-4V is presented. Fatigue variability behavior of this alloy was marked by an increase in the lifetime variability to almost three orders in magnitude as the stress level was decreased. Crack initiation was found to occur primarily from the specimen surface with only a few exceptions where subsurface initiation was recorded. In most cases, and irrespective of lifetime, crack initiation was accompanied by crystallographic facet formation across primary-□ particles. Crystallographic characterization of faceted grains and their neighborhood was conducted by sectioning across the facets using either Focused Ion Beam or mechanical polishing, and subsequent Electron Back Scattered Diffraction analysis of the sections. The emphasis in this study was on discerning the factors that distinguish the crack-initiating microstructural arrangements and plausible mechanisms producing a life-limiting failure versus a long lifetime failure under nominally similar microstructure and applied stress level.

**15. SUBJECT TERMS**

fatigue variability, crack initiation facets, Ti-6Al-4V, focused ion beam (FIB), electron back scattered diffraction (EBSD)

| 16. SECURITY CLASSIFICATION OF: | | | 17. LIMITATION OF ABSTRACT: | 18. NUMBER OF PAGES | 19a. NAME OF RESPONSIBLE PERSON (Monitor) |
|---|---|---|---|---|---|
| a. REPORT | b. ABSTRACT | c. THIS PAGE | | | Patrick Golden |
| Unclassified | Unclassified | Unclassified | SAR | 34 | 19b. TELEPHONE NUMBER *(Include Area Code)* N/A |

**Standard Form 298 (Rev. 8-98)**
Prescribed by ANSI Std. Z39-18

Approved for public release; distribution unlimited.

# Characterization of Fatigue Crack-Initiation Facets in Relation to Lifetime Variability in Ti-6Al-4V

Sushant Jha[*], Christopher Szczepanski[*], Patrick Golden, William Porter, III[#], and Reji John

Air Force Research Laboratory
AFRL/RXLMN, Materials and Manufacturing Directorate
Wright-Patterson Air Force Base, OH 45433, USA

[*]Universal Technology Corporation
1270 N Fairfield Rd., Dayton, OH 45432, USA

[#]University of Dayton Research Institute
Dayton, OH 45469, USA

## ABSTRACT

An analysis of fatigue crack-initiation facets from the perspective of variability in lifetime of a duplex microstructure of Ti-6Al-4V is presented. Fatigue variability behavior of this alloy was marked by an increase in the lifetime variability to almost three orders in magnitude as the stress level was decreased. Crack initiation was found to occur primarily from the specimen surface with only a few exceptions where subsurface initiation was recorded. In most cases, and irrespective of lifetime, crack initiation was accompanied by crystallographic facet formation across primary-$\alpha$ particles. Crystallographic characterization of faceted grains and their neighborhood was conducted by sectioning across the facets using either Focused Ion Beam or mechanical polishing, and subsequent Electron Back Scattered Diffraction analysis of the sections. The emphasis in this study was on discerning the factors that distinguish the crack-initiating microstructural arrangements and plausible mechanisms producing a life-limiting failure versus a long lifetime failure under nominally similar microstructure and applied stress level. The analyses revealed only subtle differences between the life-limiting and the long-lifetime failure in terms of deformation modes of the faceting grain(s) and their first nearest neighbors on a section. In surface crack initiation, the facets appeared to form on basal planes in

both the life-limiting and the long-lifetime failure. The subtlety of differences indicates that the facet plane and the deformation modes of the faceting grain and its neighbors in a 2D section may not be the most discriminating crack-initiation factors between the two lifetime regimes in this alloy.

**Keywords:** Fatigue variability, Crack initiation facets, Ti-6Al-4V, Focused ion beam (FIB), Electron back scattered diffraction (EBSD)

## 1. INTRODUCTION

Advanced probabilistic fatigue life-prediction methods necessitate a physics-based understanding of variability in lifetime, and, in particular, the microstructural basis of lifetime limits. Recently, several fatigue life prediction studies have focused on microstructural origins of the mean vs. the minimum lifetime [1 – 3]. In particular, it has been shown that the mean and the minimum fatigue behaviors respond at different rates to variables such as stress level, microstructure, temperature, and dwell time [1 – 3]. For example, the different rates of response with respect to the stress level leads to a separation of mean from the minimum behavior as the stress level is decreased, thereby promoting increased fatigue variability [1]. Knowledge of the local microstructure, which in many cases can be an ensemble of phases satisfying certain conditions [4], that causes the mean vs. the minimum behavior is believed to be key to not only understanding the separation of lifetimes but also to a microstructure-informed probabilistic life prediction model. Furthermore, an understanding of microstructural conditions that control the minimum fatigue behavior is useful in evaluation and design of materials for fracture critical applications.

The material of interest in the present study was Ti-6Al-4V (Ti-6-4), which is an $\alpha+\beta$ titanium alloy. Therefore, it is imperative to discuss the micro-mechanisms believed to be

pertinent to fatigue crack-initiation in α+β titanium alloys and titanium alloys in general. The α+β titanium alloys, in particular Ti-6-4, have found numerous fracture critical applications in aircraft structural components [5]. It is, therefore, not surprising that numerous studies of fatigue crack-initiation in these alloys can be found in literature. The objective here is not to present an exhaustive review of all the work that have been published on the subject but to highlight, with a few examples, the prevailing findings and theories on the micro-mechanisms of crack formation in these alloys.

A common observation across several studies on duplex microstructures of both the near-α and the α+β alloys is that fatigue crack initiation is accompanied by facet formation in globular primary-α ($\alpha_p$) particles. An earlier study by Neal and Blenkinsop [6] as well as relatively recent works of Bridier, et al. [7], Le Biavant et al [8], Germain and Bache [9], Germain, et al. [10], Dunne and Rugg [11], Sackett et al. [12], Bache, et al. [13], Pilchak et al. [14], Bantounas et al. [15], Szczepanski et al., [16], Jha et al. [1], and Jha and Larsen [4] have all reported faceted crack initiation within $\alpha_p$ particles. Additionally, Davidson and Eylon [17] and Ruppen, et al. [18], among others have reported faceted crack initiation within α/β colonies in β annealed, lamellar microstructures. Secondly, some authors have shown that faceted initiation is favored in certain microtextures or regions of common crystallographic orientation. Bridier, et al. [7], Le Biavant et al. [8], and Germain and Bache [9] reported an increased propensity for occurrence of facets in macrozones where the $\alpha_p$ grains were oriented for easy basal slip. Similarly, Szczepanski et al. [16] observed that subsurface crack initiation inTi-6-2-4-6 occurred within a microtextured region in which the α phase was suitably oriented for basal and prismatic slip. However, the facets were not uniformly distributed across the entire microtextured region but concentrated in a relatively small area (on the order of 100 μm in equivalent diameter) while the

microtextured regions were significantly larger (on the order of 500 to 1000 μm in equivalent diameter) [16]. Thirdly, in terms of the facet plane, Neal and Blenkinsop [6] suggested that the facet plane corresponds to the easy cleavage plane (believed to be the $\{10\bar{1}7\}$ plane), which makes an angle of about 14° with the basal plane. Many of the recent studies suggest that the crack-initiation facets in these alloys, in particular those resulting in dominant cracks, form on or near basal planes [7 – 16]. Crack initiation by prismatic facet formation has also been reported by some researchers [7].

Although faceted crack-initiation under fatigue has been commonly observed in titanium alloys, the suggested mechanisms of facet formation differ widely among studies. It is recognized, that some of the differences can be attributed to the specifics of alloy, microstructure, and fatigue loading regime between studies. It can also be said that the suggested mechanisms have been applicable in illuminating the fatigue – microstructure interaction under specific set of variables. However, the differing proposals across studies might also point to the scenario that a comprehensive understanding of the micro-mechanisms of facet formation in these alloys is not fully developed.

Broadly speaking, the proposed mechanisms vary in terms of the degree of contribution of cleavage versus slip in formation of the facet. As such, the mechanisms include quasi cleavage across facet plane [9, 13], the intermediate condition in which some combination of shear deformation and normal force across the facet plane is considered important [7], and those where pure slip is suggested as the most dominant factor in facet formation [14]. For example, Neal and Blenkinsop [6] suggest facet formation by cleavage across the easy cleavage plane ($\{10\bar{1}7\}$) in titanium alloys due to pile-up stresses by prismatic slip accumulation within the same α grain. Bache and coworkers [9, 13] have proposed a mechanism whereby the facet forms by quasi-

cleavage by separation across the basal plane and in which the facet plane is found to be normal to the loading axis. Bridier and coworkers [7] suggest formation of basal-plane facets by slip within $\alpha_p$ particles which do not have the maximum favorability for basal slip but are aided by sufficiently high normal stress across the slip plane. Pilchak et al. [14] showed that pure slip mechanisms were the most dominant in facet formation. In particular, they emphasized the role of slip transfer across $\alpha_p$ and $\alpha/\beta$ colony boundary where alignment of specific slip systems between the two phases produce certain residual dislocations at the boundary, promoting crack initiation [14].

The diversity of mechanisms, some of which have been reported among studies on the same alloy, also lends itself to the possibility that characterization of isolated specimens under given set of variables may not provide a complete picture in terms of the controlling mechanism. However, the study of mechanisms might be most informative if viewed in the context of the full distribution in lifetime. For example, recent studies [3, 4] on other materials have shown that an increase in the variability in lifetime can be attributed to a separation between the mean and the minimum fatigue behavior each of which are controlled by different local microstructural arrangements. An important problem, especially from the perspective of limiting lifetime prediction, might be to set the study of crack-initiation mechanism in the context of fatigue variability. The main objective of this work, therefore, was to characterize the crack-initiating microstructural configurations in the minimum or life-limiting versus the mean-fatigue lifetime specimens of Ti-6-4 under nominally similar microstructure and loading condition. The emphasis of the characterization was on crystallographic orientation and deformation modes of the faceted grain(s) and its neighbors.

## 2. MATERIAL AND METHODS

### 2.1 Material

The material in this study was the $\alpha + \beta$ titanium alloy, Ti-6-4 in a mill-annealed condition. Note that the material was obtained from forged plates that were prepared for study under the US High Cycle Fatigue Program [19]. The processing and microstructure have been reported in detail elsewhere [20, 21].The microstructure in the three orthogonal sections of the forged plate is shown in Fig. 1. As depicted, the microstructure was optically uniform in the three directions. The forged plate had a duplex microstructure, which consisted of about 60% equiaxed primary-$\alpha$ phase and 40% transformed-$\beta$ colonies. The primary-$\alpha$ size was about 20 μm on the average. The yield and tensile strength of this microstructure were reported to be 930 and 978 MPa, respectively [20, 21].

Fatigue specimen blanks were machined from the Ti-6-4 plates by electro-discharge machining (EDM). The final machining step was low stress grinding (LSG). The round-bar specimen geometry with a uniform gage section of 12.4 mm length and about 4 mm diameter was employed. The specimens were electropolished to remove approximately a 25 μm surface layer in order to provide a uniform baseline surface across specimens that is free of machining-induced imperfections and residual stresses.

### 2.2 Fatigue Experiments

Fatigue lifetime experiments were conducted in a MTS 810 servo-hydraulic test system equipped with a MTS 458 controller. The frequency of 30 Hz and the stress ratio of 0.1 were applied. Tests were done at room temperature and in the lab air. Maximum applied stress levels ranged from 600 to 750 MPa where at least 15 specimens (maximum 22) were tested at any

given stress level. All specimens were run to failure. Some specimens were utilized for small-crack growth experiments, in which the test was periodically interrupted to record surface replica, which were used to monitor crack initiation and growth.

## 2.3 Facet Characterization Method

The fracture surfaces of failed fatigue specimens were analyzed in Leica S360FE and Phillips XL30 scanning electron microscopes (SEM). The crack origin was determined by tracking the radial crack-growth pattern back to its origin, where it converged. Although in many cases the radial fracture pattern could be traced back to one or a collection of $\alpha_p$ facets, in some specimens it was not clearly apparent as to which facets can be considered as being at the origin of the crack. Those specimens may require further fractographic analysis to more conclusively discern the crack origin. Also note that for surface initiation, the crack-initiation facets were taken to be those that were at the source of the radial fracture pattern and also intersected the surface. In case of subsurface initiation, as discussed later, the origin was found to correspond to a significantly larger field of facets than seen in the surface initiation. It was not clear as to what radial distance from the origin of the faceted area could be considered as being associated with crack-initiation. Here, the facets within about 25 μm radius of the origin of the faceted area were considered as crack-initiation facets.

The characterization of crack-initiation sites, and specifically the crack-initiation facets, involved three broad steps: (i) Measurement of spatial angle of crack-initiation facets with respect to the loading axis, (ii) Sectioning across the facets, and (iii) Electron back-scattered diffraction (EBSD) analysis of the section through the facets to measure the orientation and slip modes of faceted grains and their neighbors. The measurement of facet angle was accomplished by using MEX$^{TM}$ (a trademark of Alicona Imaging GmbH), a 3D image analysis program, which

implemented a quantitative tilt microscopy method. This method has been employed in other studies for quantifying crack-initiation facet angles [4, 16]. In this, stereo-image pairs of the crack initiation site were acquired in the SEM at two different tilt angles (0 and 6° in the present study). The stereo-image pairs were used as inputs to MEX in constructing a 3D digital elevation map of the region, from which angles of facets were measured.

In the case of surface initiation, sectioning across the crack-initiation facet(s) was accomplished by focused ion beam (FIB) milling. FIB has proved to be a precise and site-specific micro-machining method with relatively high spatial resolution. In microstructural studies, FIB is further attractive due to the potential of virtually negligible machining-induced effects or deformation in the machined surface [22]. It has been employed in several materials science problems, ranging from site-specific transmission electron microscopy (TEM) foil extraction / thinning and machining of micro-meter scale tension / compression specimens in specific grains [23] to introducing micro-notches in targeted microstructural regions for small fatigue crack growth study [24].

FIB machining has also been found to be well-suited for sectioning across crack-initiation features on a fracture surface to expose the underlying microstructure for further analysis, and is beginning to be increasingly applied in fatigue crack-initiation studies [4, 14 – 16]. From the perspective of milling across crack-initiation sites, some possible limitations one might come across with the current generation of FIB tools are: (i) the speed of machining, which limits the size of the crack-initiation area that can be sectioned in reasonable time, (ii) production of curtaining marks (or parallel roughness grooves) towards the bottom end of the machined section which may obscure the microstructure, and (iii) re-deposition of sputtered material on to the

sectioned surface which, once again, may pose problems in subsequent microstructural and orientation analysis on the section.

In relatively fine microstructures, where crack initiation occurs on the scale of only a few microstructure units, the first limitation is not an issue as was the case for surface crack-initiation in the present study. Areas of about 75 μm in length and 50 μm in width were machined across surface crack-initiation facets, which allowed the characterization of faceted $\alpha_p$ particles and their first nearest neighbors in the section. The accelerating voltage of 30 kV and the ion beam current of about 6.5 nA were employed. The milling process was constantly monitored by periodically capturing an electron image of the milled surface. Since facets in subsurface-initiation occurred over a much larger area than in surface initiation, mechanical polishing was used to section through the subsurface crack-initiation site. It is, however, believed that localized sections across individual facets using FIB in conjunction with mechanical sectioning will be very useful in maximizing the number facets analyzed in a large subsurface crack initiation site in an efficient manner.

The second limitation, i.e., the curtaining effect may occur during any cross-section machining using an ion beam [22] and is believed to be associated with variable sputter yields related to varying surface curvature. This effect may limit the width of the region that has a smooth surface for future microstructural analysis. However, the curtaining issue might be minimized by machining at different angles (which was not implemented in this study) but also by limiting the total machining time.

The re-deposition effect will prevent good patterns in an electron back-scatter diffraction (EBSD) scan. One method to mitigate this issue is to incorporate a low kV cleaning as the final milling step [14]. A broad-beam Argon milling as a cleaning step after FIB milling has also been

proposed, and shown to be effective in removing the re-deposited layer in some cases [25]. One approach that was found useful in this study was to optimize the total milling time by maintaining a balance between the beam size (a coarser beam can produce poorer surface from the perspective of EBSD analysis) and time of milling. A shorter time was found to minimize the re-deposition effect while also being helpful in reducing the area affected by curtaining marks.

The third step in the characterization procedure was to conduct EBSD analysis of the FIB section in order to measure the orientation and slip modes of the faceted grains and their first nearest neighbors. This was accomplished by a Hikari EBSD camera installed on a Phillips XL30 SEM which had a maximum frame rate of about 440 frames per second. The EDAX-TSL data collection program was used for acquiring EBSD data. The subsequent EBSD data analysis was performed with the EDAX-TSL data analysis program.

## 3. RESULTS AND DISCUSSION

### 3.1 Fatigue Lifetime Variability

The fatigue variability behavior of Ti-6-4 in the mill-annealed microstructural condition has been reported previously [20] and is shown in Fig. 2. All data points in the figure represent failure. The surface and subsurface crack-initiation are shown by open and closed symbols, respectively. As expected, the mean lifetime showed a significantly increasing trend with decreasing stress level, varying from about 6 X $10^4$ cycles to about $10^7$ cycles within the range of stresses (between 750 and 600 MPa) considered in this study. Simultaneously, with decreasing stress level, a significant increase in the variability in lifetime was also observed such that lifetimes varied by almost three orders in magnitude at the lowest applied stress level of 600 MPa. It is also apparent that the life-limiting failures, i.e., the short lifetime population with

lifetimes on the order of $10^5$ cycles, showed a trend which was very disparate from that of the mean behavior as a function of stress level. This, separation of mean from the life-limiting behavior, has been reported in previous studies [1 – 4] including those on the $\alpha+\beta$ titanium alloy, Ti-6Al-2Sn-4Zr-6Mo and is suggested to be the primary contributor to the increased variability in lifetime as the stress level is decreased. Note that only two subsurface-initiated failures were observed in the given number of tests. Although subsurface crack initiation was associated with longer lifetimes than the surface initiation, the divergence between mean and life-limiting behaviors was independent of the occurrence of subsurface failures.

Possible physical underpinnings of the separation of the mean and the life-limiting fatigue behavior and its implications in probabilistic life prediction have been discussed elsewhere [1]. Here, the goal was to characterize the local microstructures associated with crack-initiation in the life-limiting versus the mean-lifetime populations in an effort to elucidate the respective mechanisms. Three specimens were selected for this purpose, which are indicated in Fig. 2 by dashed squares. A surface-initiated failure was selected from each of the two populations. In addition, a subsurface failure was also selected. Both surface-initiation specimens were run at 630 MPa and represented the minimum and the maximum lifetime ($N_f$ of 106,935 and 3,063,865 cycles, respectively) at that stress level. The subsurface-initiation specimen was run at 600 MPa and had the longest lifetime ($N_f$ = 76,110,019 cycles). The crack-initiation sites in these three specimens were characterized by the methods described in section 2 and the results are presented in the following.

### 3.2 Crack-Initiation Characteristics in Life-Limiting and Long-Lifetime Failures

*Life-limiting failure*: Details such as test condition, lifetime, and the crack-initiation characteristics in the three selected specimens are provided in Table I. The specimen from the

life-limiting population was run at 630 MPa and failed by surface crack-initiation with the lifetime of 106,935 cycles. An overview of the crack-initiation region is shown in a low magnification secondary electron image in Fig. 3(a). As seen in this figure, the crack origin can be traced to a flat, featureless facet at the specimen surface. As discussed earlier, the crack-initiation facet(s) in surface failures was considered as the facet or a group of facets that were traced to the crack origin and intersected the surface of the specimen. A higher magnification image of the suggested crack-initiation facet is presented in Fig. 3(b). The size and shape of the facet, labeled as F1, were similar to that of a $\alpha_p$ particle. The spatial angle of the facet-normal with respect to the loading axis, measured using MEX, was about 30° (Table I). The facet was therefore, not oriented for maximum shear deformation.

A section was milled across the crack-initiation facet using FIB, as shown in Fig. 4(a). The section was made normal to the fracture surface. The $\alpha_p$ particle which produced the facet is indicated in the figure (labeled as F1). The first nearest $\alpha_p$ particles and the $\alpha/\beta$ colonies, which are designated as N1 to N7, have also been labeled in Fig. 4(a). Note that the image in Fig. 4(a) was captured at a 30° tilt in the SEM in order to simultaneously reveal the fracture and the milled surfaces. Therefore, the microstructural dimensions appear distorted in the tilt direction in this image.

The Inverse Pole Figure (IPF) map of the FIB section (Fig. 4(a)) obtained by the EBSD analysis is presented in Fig. 4(b). The IPF map has been referenced such that the crystallographic orientations are shown in the loading direction. The faceted $\alpha_p$ and its neighbors are, once again, labeled in the IPF map. The hexagonal lattice and the basal plane trace are depicted for the faceted grain. As shown in Fig. 4(b), the basal plane trace of the faceted grain demonstrated good correspondence to the facet trace. The Inverse Pole Figures (IPF) corresponding to the EBSD

data for the crack-initiating $\alpha_p$ particle and the neighboring grains are presented in Fig. 4 (c) and (d), respectively. In the IPF, the loading directions in the grains of interest are plotted in the crystal reference frame. The shaded areas in Fig. 4(c) and (d) and the IPFs shown in later figures in this paper represent, from left to right, regions of high Schmid Factor (SF) for basal <a>, pyramidal <a>, and prismatic <a> slip.

As stated above, the angle of the crack initiation facet-normal to the loading axis in the life-limiting specimen was about 30°, therefore, not oriented for maximum shear. However, Fig. 4(c) indicates that the faceted grain in this specimen was close to being favorably oriented for basal slip, where the SF was about 0.44. This, in conjunction with the result that the basal plane trace corresponded to the facet trace (Fig. 4(b)), points to a strong likelihood that the facet represents either the basal plane or a plane very close to the basal plane. However, since the facet plane was not oriented for maximum shear it can be suggested that a combination of basal slip and stress component normal to the basal plane produced the facet, similar to the mechanism proposed by Bridier, et al. [7].

The first nearest neighbors (on the FIB section) of the faceted $\alpha_p$, identified in Fig. 4(a) and (b), consisted of both the equiaxed $\alpha_p$ particles as well as the $\alpha/\beta$ colonies. The crystal orientations in the neighboring grains along the loading direction are plotted on the IPF in Fig. 4(d) where $\alpha_p$ and colony are represented by different symbols. The IPF suggests that most of the neighboring $\alpha_p$ and $\alpha$ laths were favorably oriented for either basal <a> or prismatic <a> slip. Note however, that only the neighbors intersected by a 2D section are plotted here, and it is not clear if the same result will be obtained if the full 3D neighborhood was characterized. Nevertheless, it appears that in this life-limiting specimen the facet plane was basal or close to

basal and its formation was aided by basal slip as well as normal stress across the facet plane. Further, based on a 2D characterization, the neighbors to the faceted $\alpha_p$ appear to be close to favorably oriented for either basal or prismatic slip.

*Long-lifetime failure*: The specimen selected from the long-lifetime failure population was tested at the same stress level ($\sigma_{max}$ = 630 MPa) as the previously discussed life-limiting specimen. The specimen failed from surface crack-initiation and had the lifetime of 3,063,865 cycles. An overview of the crack initiation region and a higher magnification SEM image showing the suggested crack-initiation facets are presented in Fig. 5 (a) and (b), respectively. The crack origin could be traced back (using radial crack growth pattern) to a group of three facets that intersected the surface (Fig. 5(b)), which are suggested to be the crack-initiation facets. These are labeled as F1 to F3 in the figure. Again, the crack initiation facets were considered to be those that were at the area of convergence of the radial fracture pattern and also intersected the specimen surface. Since it consists of multiple facets, the crack-initiation area in this case appears larger than in the life-limiting specimen discussed before in spite of more than an order of magnitude longer lifetime. This further emphasizes the significance of crystallographic deformation modes of crack-initiating grains and their neighborhood in affecting crack initiation and lifetime.

The facet angles of the three suggested crack-initiation facets, F1, F2, and F3 were 41, 56, and 44°, respectively. Therefore, in this case, the facets are closer to being oriented for maximum shear. The results from crystallographic analysis of facets and their neighborhood are presented in Fig. 6. The FIB section milled across the three facets is shown in the tilted SEM image in Fig. 6(a). The crack-initiation facets are labeled on the fracture and the milled surfaces and the first nearest neighboring grains, labeled as N1 to N8, are indicated on the FIB surface. It can be

clearly seen from Fig. 6(a) that the suggested crack-initiation facets formed in $\alpha_p$ particles. The IPF map corresponding to the FIB section is presented in Fig. 6(b). The hexagonal lattice and the basal plane trace have been included for the faceted grains. The basal plane trace in each of the three faceted grains had close correspondence to the respective facet plane trace, as shown. The IPF plotting the crystallographic orientations of faceted $\alpha_p$ along the loading axis is presented in Fig. 6(c). The figure shows that the faceted $\alpha_p$ particles were close to a favorable orientation for basal slip with SF of 0.45, 0.46, and 0.47.

The orientation of neighboring $\alpha_p$ particles and colonies, marked in Fig. 6(b), are plotted in the IPF shown in Fig. 6(d). The figure indicates that the neighboring grains on the FIB section did not have preference for any specific slip mode or modes but seem to be distributed across the orientation space. The neighbors to the crack-initiation facets in the long-lifetime case, therefore, appear to be different than those in the life-limiting failure but considering that only those neighbors intersected by a 2D section are represented in Fig. 5(d) and 6(d), it is not clear if these differences are significant contributors to the wide disparity in lifetime.

Although 2D section across crack-initiation facets has been analyzed, it seems that in the long-lifetime specimen the facet formation involved a stronger contribution from basal slip since the facets were oriented for close to maximum shear deformation. Therefore, it appears that in the present long-lifetime specimen, facet formation by a basal slip assisted crack nucleation mechanism is applicable. Additionally, the role of the neighborhood of crack-initiation facets is not apparent when a set of all nearest neighbors on a section are considered. However, it is possible that in this case only a subset of nearest neighbors, those that are along the slip band,

play a role in terms of slip transfer behavior as proposed by Pilchak, et al. [14] in promoting crack nucleation along the slip band.

*Subsurface initiation*: As shown in Fig. 2, only two subsurface initiated failures were observed in the given number of tests. Both of these failures occurred at the stress level, $\sigma_{max}$ of 600 MPa, which was the lowest stress level considered in this study. The lifetimes of subsurface failures were longest among specimens in the long-lifetime population. The specimen selected for characterization had the lifetime of 76,110,019 cycles. The subsurface crack origin was marked by a significantly larger area, compared to surface crack initiation, over which facets were formed as illustrated by Fig. 7. An overview of the crack initiation area is shown in Fig. 7(a) where a large field of facets is seen at the convergence of radial fracture pattern. Due to subsurface initiation and the large crack-initiation area, FIB milling was not the most suitable technique to section across the facets. Therefore, in this case, the sectioning was done by mechanical polishing. It is useful to note that although the sectioning plane, indicated in Fig. 7(a), passed through the region of maximum density of facets it did not intersect the center of crack initiation area. A higher magnification image of the subsurface crack origin is presented in Fig. 7(b) where the facets have been labeled. The spatial angle of facets with respect to the loading axis ranged from about 20 to 74°. The wide range in facet angles can be attributed to the fact that some of the facets that were characterized may not be crack-initiation facets but could have formed during small-crack growth. The distribution in facet angles, illustrated by the histogram in Fig. 7(c), indicates that a majority of facets were oriented between 30 and 60° with respect to the loading axis. Therefore, most of the facets in subsurface initiation can be considered to be suitably oriented for shear deformation mode.

Crystallographic analysis of the faceted grains and their neighborhood is presented in Fig. 8. The mechanical section intersected some of the facets as shown in Fig. 8 (a), where the facets have been indicated on the fracture surface and the section. All the facets intersected by the sectioning plane appear to have formed within $\alpha_p$ particles. The IPF map of the section is shown in Fig. 8(b). The plane traces and the crystal lattice for the faceted $\alpha_p$ particles, identified in the figure, have been included. In this case, some facet plane traces were found to correspond to the prismatic plane trace while others aligned with the basal plane trace, as shown. This is different from surface crack initiation facets where all crack initiation facet traces corresponded to close to the basal plane traces. It is, however, not clear if all the facets intersected by the sectioning plane in the subsurface initiation specimen were crack-initiation facets. Therefore, the fact that a specific plane trace is not observed can be attributed to the likelihood that all facets on this section cannot be considered as crack initiation facets.

The crystal orientations in the faceted grains along the loading axis are plotted in the IPF shown in Fig. 8(d). As expected from the plane trace analysis, not all faceted $\alpha_p$ particles on the section were favorably oriented for basal slip but some were also oriented for prismatic and even pyramidal slip. Although it is not clear which facets were formed in the crack initiation stage, from the plane trace analysis and the IPF, it can be suggested that most of the facets appear to have formed along low index slip planes.

The crystal orientation of first nearest neighbors of the faceted grains have been plotted in Fig. 8(d). The neighboring $\alpha_p$ particles and colonies plotted across the orientation space without showing preference for specific deformation modes. This might point to a stronger influence of neighbors that are in the path of the slip band in promoting crack initiation. It can be speculated

that in subsurface initiation a significantly larger microstructural arrangement (compared to surface initiation) is required where the $\alpha_p$ particles in the arrangement and those neighbors which are along the slip bands satisfy certain slip conditions.

## 4. CONCLUSIONS

The following main conclusions can be drawn from this study:

(i) Fatigue variability behavior of the duplex Ti-6-4 alloy was marked by different trends of the mean and the life-limiting fatigue response with respect to the stress level.

(ii) Crack-initiation occurred by facet formation in $\alpha_p$ particles in both the life-limiting and the long-lifetime (which dominated the mean behavior as the stress level was decreased) failures.

(iii) In the selected life-limiting specimen, the crack initiation occurred in the specimen surface and the facet-normal was oriented at about 30° with respect to the loading axis. The crystallographic analysis of the faceted $\alpha_p$ suggested a strong likelihood of the facet plane being the basal or near basal plane. The first nearest neighboring grains (on a section) to the facets were found to be favorably oriented for easy slip modes, i.e., basal and prismatic slip. Facet formation by a combination of slip and resolved normal force across the facet plane can be suggested as a possible crack initiation mechanism in this case.

(iv) In the selected long-lifetime specimen that failed by surface crack-initiation, more than one facets were identified to be associated with crack initiation. The facet angles in this case ranged between 41 – 56° with respect to the loading axis. The SF and plane trace analyses suggested a strong likelihood that the facet planes

corresponded to the basal plane. The neighborhood of faceted grains did not show a preference for any specific slip mode. It can be suggested that in the long-lifetime specimen, shear deformation coupled with the role, in terms of slip transfer characteristics, of those neighbors that were in the path of the slip band in the faceted $\alpha_p$ particles was a more dominant mechanism of facet formation.

(v) In the subsurface-initiated failure facets occurred over a significantly larger area than in the surface crack initiation. The facet angles ranged from 20 – 74° although the majority of facets were inclined between 30 – 60° with reference the loading axis. It was not clear which facets were associated with crack initiation but some faceted $\alpha_p$ particles were found to be favorably oriented for basal slip, while others were oriented for prismatic slip, and some for pyramidal slip. The facet planes appeared to correspond to low index slip planes. The neighboring phases to the faceted $\alpha_p$ did not display a specific crystallographic deformation mode.

(vi) In spite of some differences, in terms of crystallographic characteristics, between the crack-initiation arrangements in the life-limiting and the long-lifetime specimen, it is not clear if these differences are significant contributors in producing the wide variability in lifetime. It is possible that in addition to these crystallographic differences, other factors such as alignment of slip across interfaces, chemical inhomogeneity, etc., which are not captured in the present study, might be more discerning between the life-limiting and the long-lifetime failures. Also to be noted is that the role of the crack-initiation facet neighborhood in facet formation might be more clearly determined by an analysis of the 3D volume around the facets.

**Acknowledgements**

This work was performed at the Air Force Research Laboratory, Materials and Manufacturing Directorate, AFRL/RXLMN, Wright Patterson Air Force Base, OH. The partial financial support of the Air Force Office of Scientific Research, Dr. David Stargel, Program Manager, is gratefully acknowledged. Three of the authors were partially supported under onsite Air Force contracts FA8650-07-D-5800 (SKJ and CJS) and FA8650-09-C-5223 (WJP).

**References**

[1] S.K. Jha, J.M. Larsen and A.H. Rosenberger, *Engineering Fracture Mechanics*, Vol. 76, pp. 681-694, 2009.

[2] S.K. Jha, M.J. Caton and J.M. Larsen, *Materials Science and Engineering A*, 468-470, pp. 23-32, 2007.

[3] S.K. Jha, M.J. Caton and J.M. Larsen, *Superalloys 2008*, Eds. R. C. Reed etc, Sept. 14-18 2008, Champion, PA TMS, pp. 565-572, 2008.

[4] S.K. Jha and J.M. Larsen, *VHCF-4, Proceedings of the Fourth International Conference on Very High Cycle Fatigue*, pp. 385-396, 2007.

[5] R. R. Boyer, *Materials Science and Engineering A*, Vol. A213, pp. 103-114, 1996.

[6] D. F. Neal and P. A. Blenkinsop, *Acta Metallurgica*, Vol. 24, pp. 59-63, 1976.

[7] F. Bridier, P. Villechaise, and J. Mendez, *Acta Materialia*, 56, 3951-3962, 2008.

[8] K. Le Biavant, S. Pommier, and C. Prioul, *Fatigue Fract Engng Mater Struct*, Vol. 25, pp. 527-545, 2002.

[9] L. Germain and M. R. Bache, in *Ti 2007, Proceedings of the 11$^{th}$ World Conference on Titanium*, Eds. M. Niinomi, S. Akiyama, M. Hagiwara, M. Ikeda and K. Maruyama, Kyoto, Japan, pp. 953-956, 2007.

[10] L. Germain, E. E. Sackett, and M. R. Bache, in *Ti 2007, Proceedings of the 11$^{th}$ World Conference on Titanium*, Eds. M. Niinomi, S. Akiyama, M. Hagiwara, M. Ikeda and K. Maruyama, Kyoto, Japan, pp. 271-274, 2007.

[11] F. P. E. Dunne and D. Rugg, *Fatigue Fract Engng Mater Struct*, Vol. 31, 949-958.

[12] E. E. Sackett, L. Germain, and M. R. Bache, *Int J Fatigue*, Vol. 29, pp. 2015-2021, 2007.

[13] M. R. Bache, W. J. Evans, and H. M. Davies, *J Mater Sci*, Vol. 32, pp. 3435-3442, 1997.

[14] A. L. Pilchak, R. E. A. Williams, and J. C. Williams, *Metall and Mater Trans A*, Vol. 41A, pp. 106-124, 2010.

[15] I. Bantounas, D. Dye, and T. C. Lindley, *Acta Materialia*, Vol. 58, pp. 3908-3918, 2010.

[16] C.J. Szczepanski, S.K. Jha, J.M. Larsen and J.W. Jones, *Metallurgical and Materials Transactions A*, Vol. 39A, December, pp. 2841-2851, 2008.

[17] D. L. Davidson and D. Eylon, *Metall Trans A*, Vol. 11A, pp. 837-843, 1980.

[18] J. A. Ruppen, D. Eylon, and A. J. McEvily, *Metall Trans A*, Vol. 11A, pp. 1072-1075, 1980.

[19] Advanced High Cycle Fatigue (HCF) Life Assurance Methodologies, Report, AFRL-ML-WP-TR-2005-4102, July 2004, Wright-Patterson Air Force Base, Ohio.

[20] P. J. Golden, R. John, and W. J. Porter, III, *Procedia Engineering*, Vol. 2, pp. 1839-1847, 2010.

[21] M. A. Moshier, T. Nicholas, and B. M. Hillberry, in ASTM-STP 1417, pp. 129-146, 2002.

[22] N. Mateescu, M. Ferry, W. Xu, and J. M. Cairney, *Materials Chemistry and Physics*, Vol. 106, pp. 142–148, 2007.

[23] L. A. Giannuzzi and F. A. Stevie, *Micron*, Vol. 30, pp. 197–204, 1999.

[24] M. J. Caton, R. John, W. J. Porter, and M. E. Burba, *International Journal of Fatigue*, accepted for publication, 2010.

[25] Personal communication with Robert Wheeler, UES Inc.

Table I: Characteristics of suggested crack-initiation facet(s) in selected specimens of Ti-6-4.

| **Designation** | **$\sigma_{max}$ (MPa)** | **$N_f$ (Cycles)** | **Crack origin** | **Facet angle (°)** | **SF for basal slip** | **Likely facet plane** |
|---|---|---|---|---|---|---|
| Life-limiting | 630 | 106,935 | Surface | 30 | 0.44 | Basal |
| Long-lifetime | 630 | 3,063,865 | Surface | 41 – 56 | 0.45 – 0.47 | Basal |
| Subsurface initiation | 600 | 76,110,019 | Subsurface | 20 – 74 | | Basal, prismatic |

**Figures**

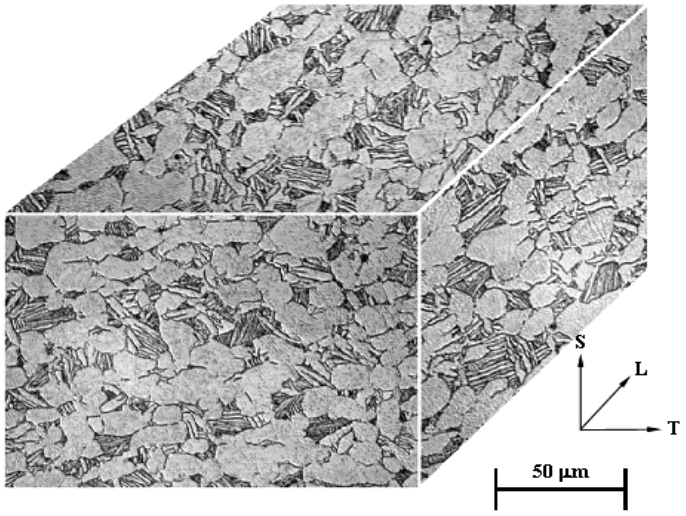


Fig. 1: Microstructure of the Ti-6-4 alloy employed in the present study.

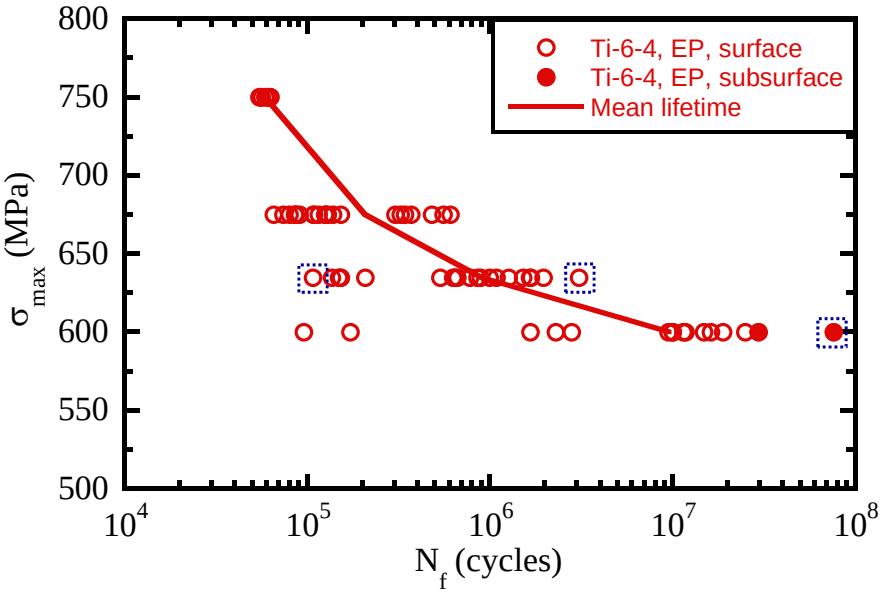


Fig. 2: Fatigue variability behavior of Ti-6-4. The dashed squares indicate the specimens that were selected for characterization of the crack initiation site.

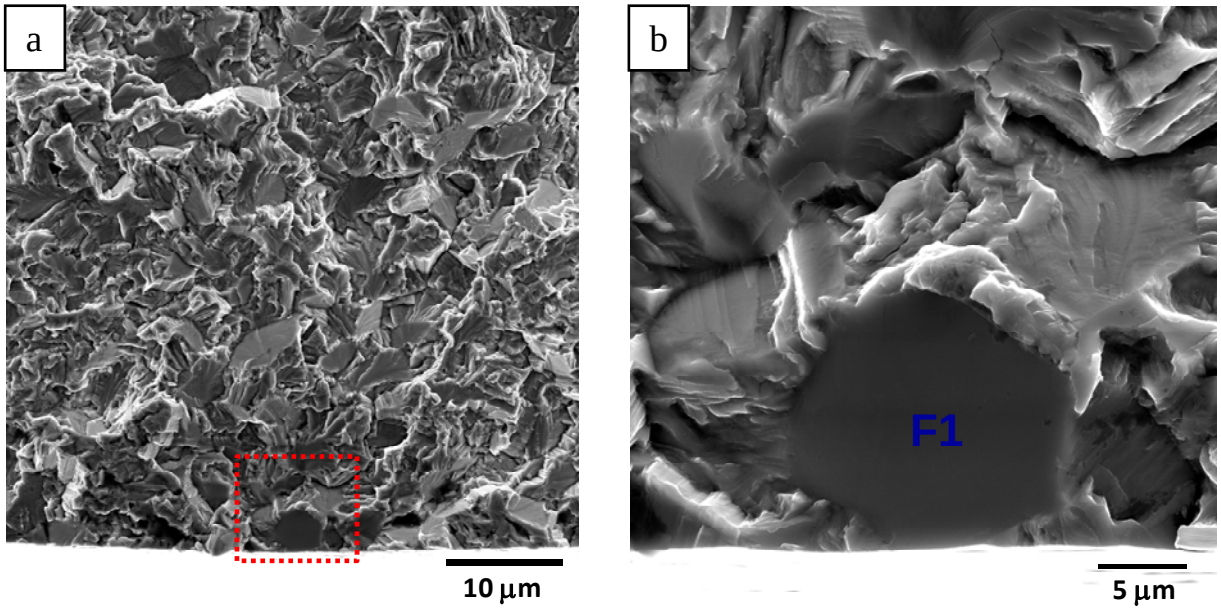


Fig. 3: Crack-initiation in the life-limiting specimen tested at 630 MPa with the lifetime of 106,935 cycles; (a) the crack-initiation region and (b) the suggested crack-initiation facet.

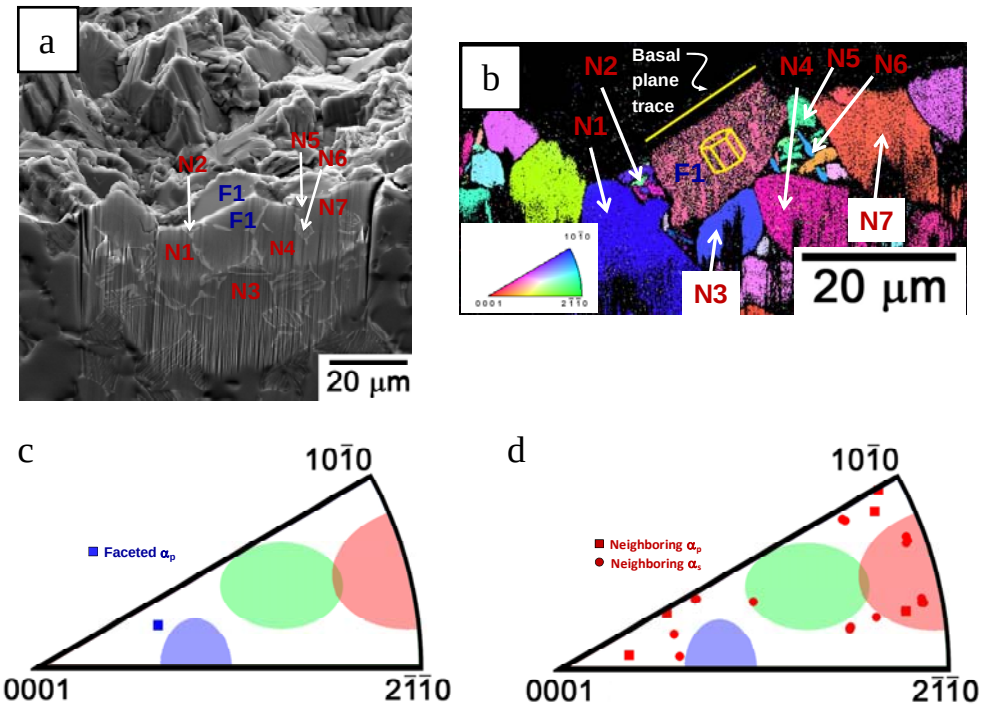


Fig. 4: Characterization of crack-initiation facet and neighboring phases in the life-limiting specimen. (a) The FIB section across the crack-initiation facet. The faceted $\alpha_p$ is labeled as F1 and the first nearest neighbor grains are labeled from N1 to N7; (b) The IPF map obtained by EBSD analysis of the FIB section; (c) The IPF showing the loading direction in the faceted grain in the crystal reference frame. The shaded areas correspond to, from left to right, the regions of high SF for basal <a>, pyramidal <a>, and prismatic <a> slip respectively; (d) The IPF, plotting the first nearest neighboring $\alpha_p$ and colonies on the FIB section.

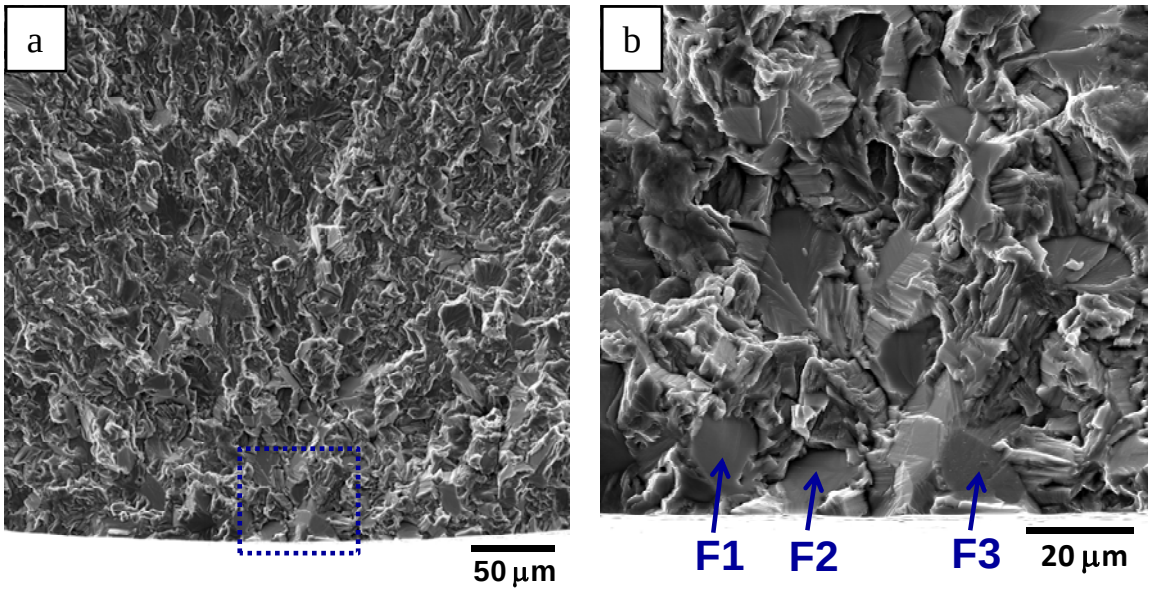

Fig. 5: Crack-initiation in the long-limiting specimen tested at 630 MPa with the lifetime of 3,063,865 cycles; (a) the crack-initiation region and (b) suggested crack-initiation facets.

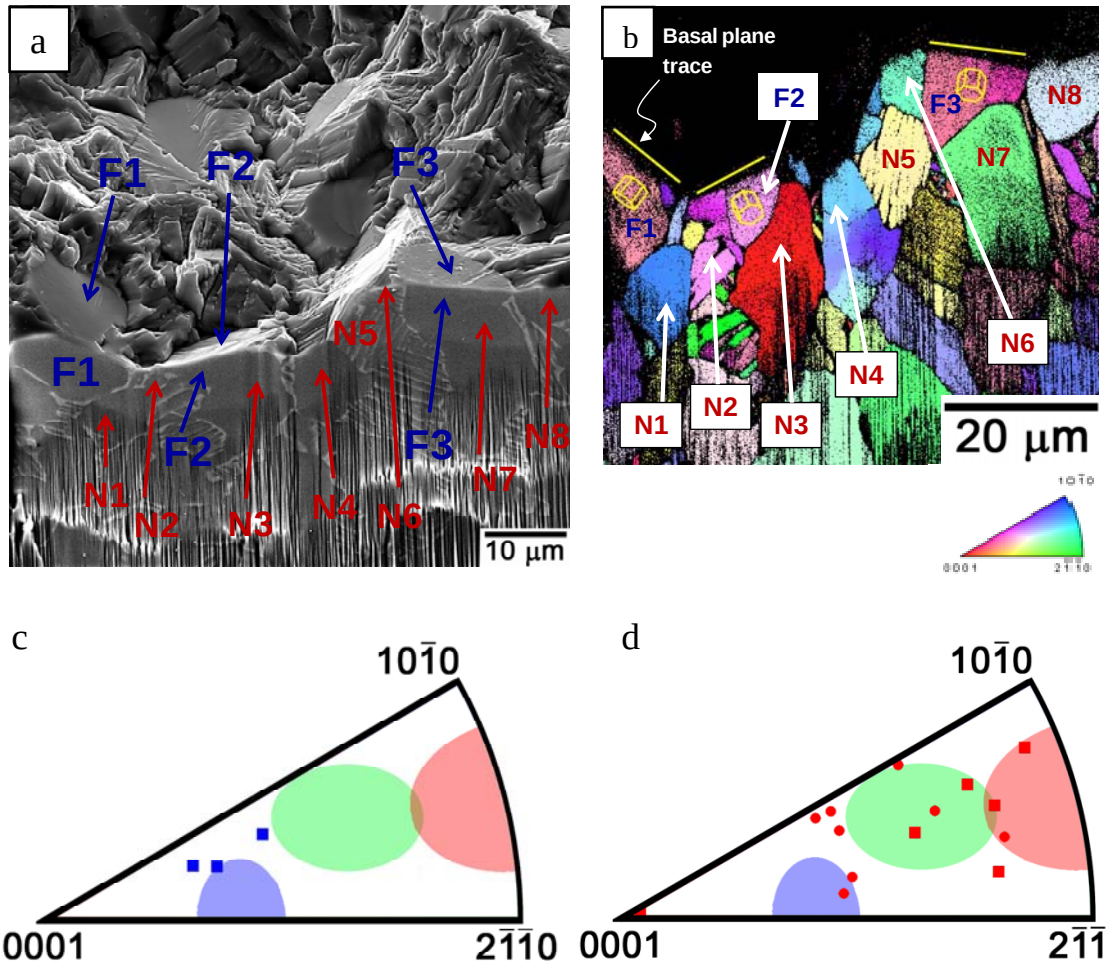


Fig. 6: Characterization of crack-initiation facet and neighboring phases in the long-lifetime specimen. (a) The FIB section across the crack-initiation facets. The faceted $\alpha_p$ particles are labeled as F1 to F3 and the first nearest neighbor grains are labeled from N1 to N8; (b) The IPF map obtained by EBSD analysis of the FIB section; (c) The IPF showing the loading direction in the faceted grain in the crystal reference frame. The shaded areas correspond to, from left to right, the regions of high SF for basal <a>, pyramidal <a>, and prismatic <a> slip respectively; (d) The IPF, plotting the first nearest neighboring $\alpha_p$ and colonies on the FIB section.

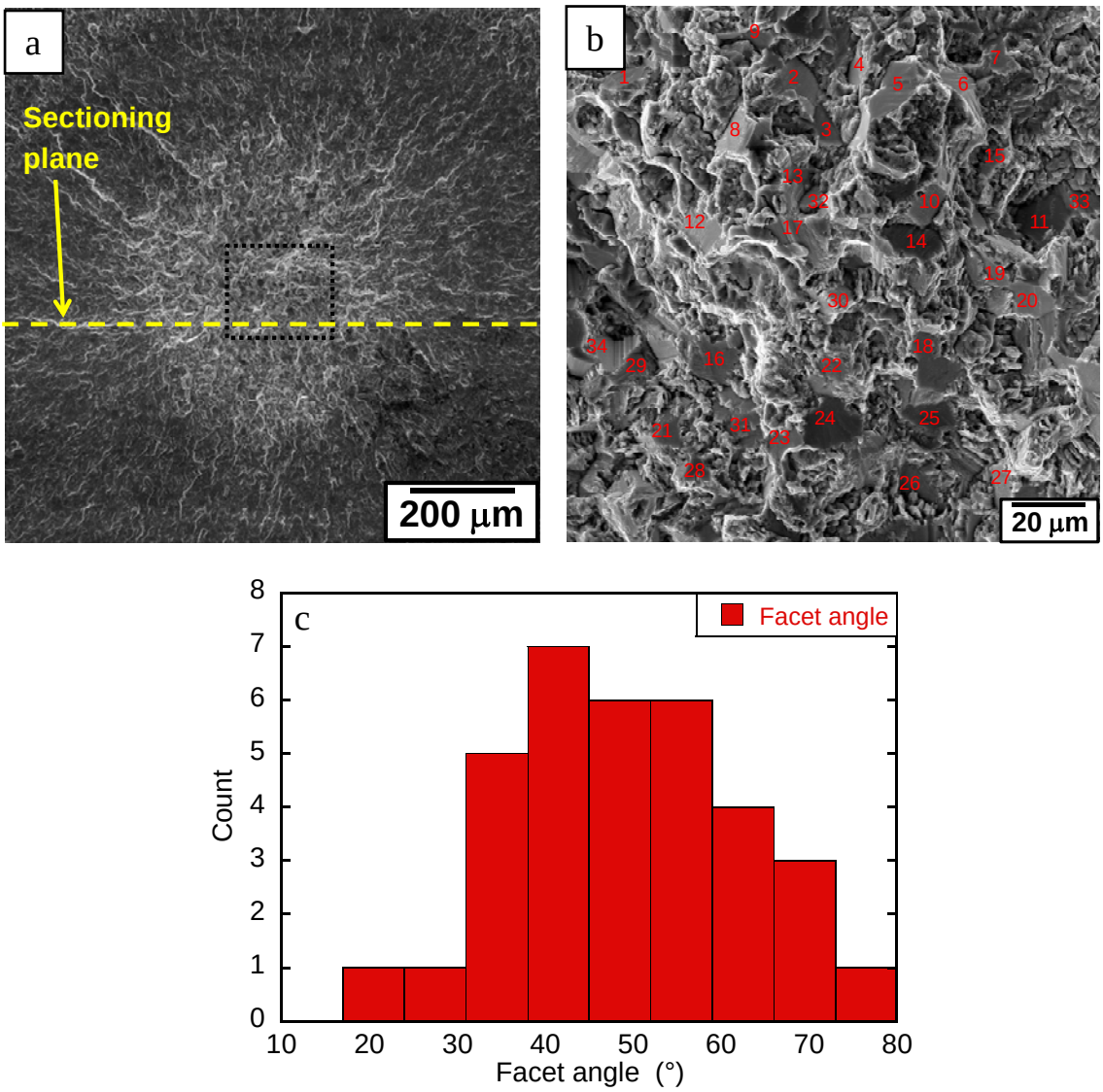


Fig. 7: Crack-initiation in the subsurface crack-initiation specimen tested at 600 MPa with the lifetime of 76,110,019 cycles; (a) the crack-initiation region, (b) facets near the crack origin, and (c) distribution in spatial angle of facets identified in (b).

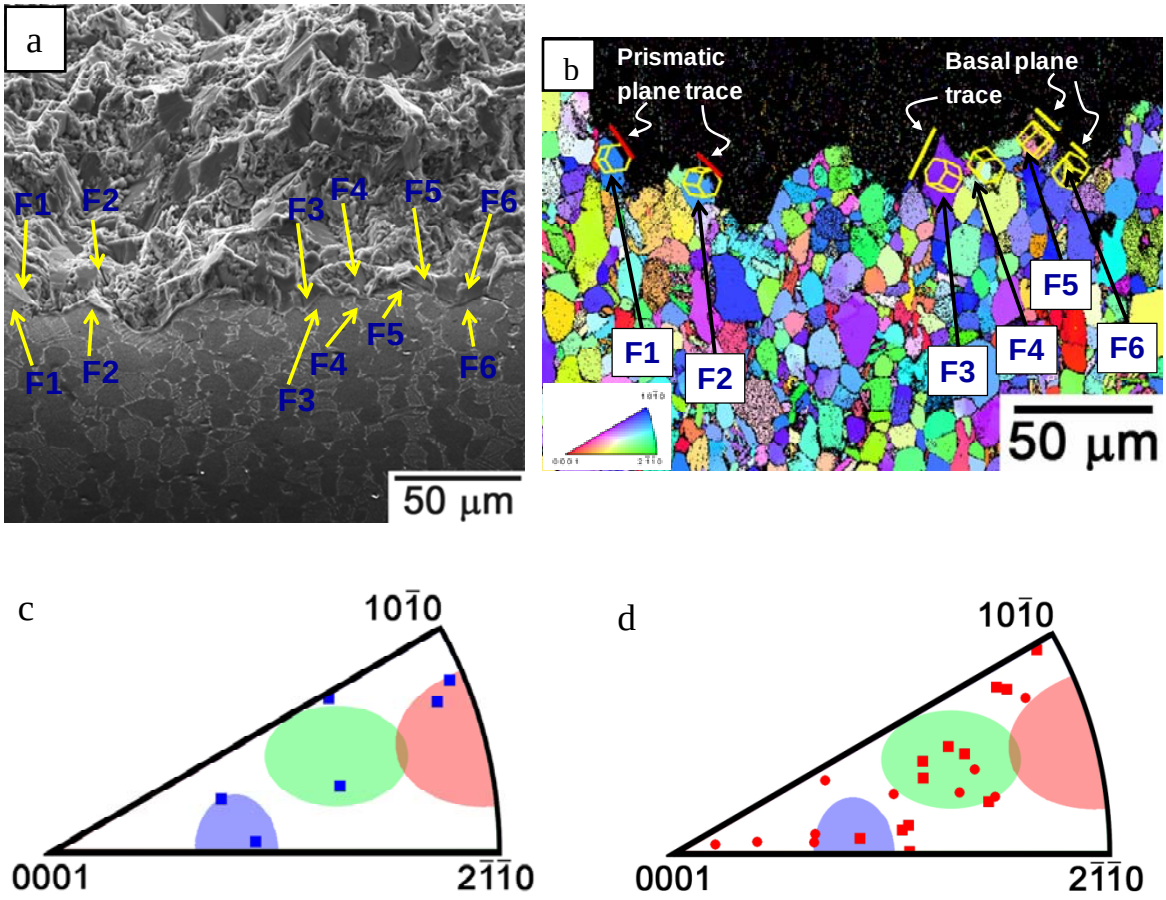


Fig. 8: Characterization of facets near the crack origin and the neighboring phases in the subsurface crack-initiation specimen. (a) The mechanically-polished section near the crack initiation site. The faceted $\alpha_p$ particles intersected by the section are labeled as F1 to F6; (b) The IPF map obtained by EBSD analysis of the section; (c) The IPF showing the loading direction in the faceted grain in the crystal reference frame. The shaded areas correspond to, from left to right, the regions of high SF for basal <a>, pyramidal <a>, and prismatic <a> slip respectively; (d) The IPF, plotting the first nearest neighboring $\alpha_p$ and colonies on the section.